Multibit Programmable Optoelectronic Nanowire Memory with Sub-femtojoule Optical Writing Energy

Ming-Pei Lu, Ming-Yen Lu, and Lih-Juann Chen*

Persistent challenges in the nanofabrication of optoelectronic memory elements with ready size-scalability, multibit data storage, and ultralow optical writing energy have limited progress toward the construction of optical data storage/buffering elements in high-density photonic-electronic circuits. Here, a multibit programmable optoelectronic nanowire (NW) memory is described that operates with an ultralow optical writing energy [ca. 180 aJ bit^{-1} (ca. 330 photons bit^{-1})] and a low standby power consumption (<1 pW) at room temperature. In this system, photoionized charged defects behave as surface trapped charges to achieve the electrical memory effect. As a result of the high surface electric field, the rate of dissociation of the photoexcited charge is amplified, thereby decreasing the optical writing energy. Moreover, the extremely high dynamic photoconductive gain (ca. 10^{10}) makes it possible to write multibit optical data bit-by-bit into the NW. These findings should open new opportunities in next-generation multifunctional nanochips for optical data storage/buffering, optical data processing, and optical sensing purposes.

1. Introduction

Developing nano-structured technologies for the integration of photonics into electronics on the nanometer scale will enable the preparation of highly integrated nanochips exhibiting great functionalities and having promising applications in areas ranging from optical interconnections to optical computing and communications.[1] One-dimensional nanomaterials having high aspect ratios and significant surface effects have been proposed as key elements (e.g., nanoscale lighting sources,[2] optical switches,[3] photodiodes,[4] photovoltaic devices,[5] waveguides[6] for the feasible production of 3D multifunctional photonic circuits schemed using high-density nanoscale interconnects. Furthermore, to meet the demands of an optoelectronic memory element for optical data storage/buffering, hybrid integration technologies combining photoactive organic molecules and nanostructured materials have been used to prepare optoelectronic memories.[7] Nevertheless, considerable difficulties in integrating hybrid devices into highly integrated nanochips must be resolved if they are to find practical applications.

The internal phenomenon of persistent photoconductivity (PPC)—that is, photoconductivity persisting for a long time after termination of optical excitation—originates from the slow recovery of the atomically photoinduced structural transition of certain defect centers with large lattice relaxation; it has been investigated extensively over 40 years in many semiconductors, including compound semiconductors, metal oxides, and chalcopyrite materials.[8–12] Only a few studies have attempted to exploit the PPC effect to realize two-level optoelectronic thin film memories without a photoactive organic coating;[13] the resulting optical writing energy of a few microjoules has, however, been several orders of magnitude greater than the sub-femtojoule switching energy of state-of-the-art Si logic transistors possessing sub–100 nm feature sizes.[14] The ability to greatly decrease the optical writing energy appears to be the most important challenge affecting the development of optoelectronic memory technologies for use in future photoelectronic applications.

Here, we demonstrate a multibit programmable optoelectronic memory featuring an ultralow optical writing energy [ca. 180 aJ bit^{-1} (ca. 330 photons bit^{-1})] and a low standby power consumption (<1 pW) at room temperature, prepared using an n-type ZnO nanowire field-effect transistor (NWFET); this approach has promise for the development of optoelectronic memory elements for use in nano-photonic-electronic circuits. The positively charged defects formed upon photoexcitation can be used as surface trapped charges to induce electrical memory effects in NW memories. The resulting high electric field within the surface space-charge layer enhances the dissociation rate of the photoexcited charges. Our observation of an ultrahigh dynamic photoconductive gain (ca. 10^{10}) enabled a memory capacity for writing optical data bit-by-bit into an NW. Moreover, the presence of the significant PPC effect in the ZnO NW favors the retention of photoconductive characteristics for electrical reading at each optical bit.

Dr. M.-P. Lu
National Nano Device Laboratories
National Applied Research Laboratories
Hsinchu, 30078, Taiwan
E-mail: mingpei.lu@gmail.com; mplu@narlabs.org.tw
Prof. M.-Y. Lu
Graduate Institute of Opto-Mechatronics
National Chung Cheng University
Chia-Yi, 62102, Taiwan
Prof. L.-J. Chen
Department of Materials Science and Engineering
National Tsing Hua University
Hsinchu, 30043, Taiwan

DOI: 10.1002/adfm.201303864

© 2014 WILEY-VCH Verlag GmbH & Co. KGaA, Weinheim

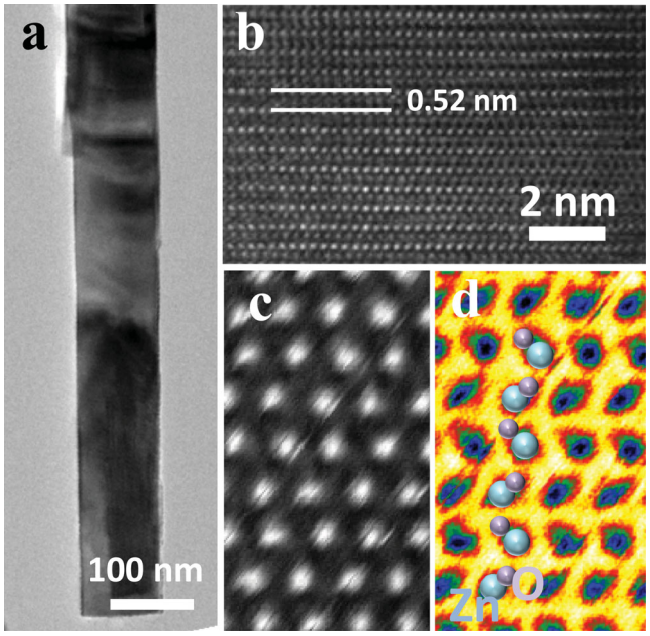

Figure 1. (a) Low-magnification TEM image of a ZnO nanowire. (b) HRTEM image of a ZnO NW, revealing the lattice spacing of 0.52 nm corresponding to the (0001) plane of ZnO. (c) Annular dark field (ADF) and (d) annular bright field (ABF) STEM images of a ZnO NW; the ABF STEM image reveals the ABAB stacking order of a wurtzite structure.

2. Results and Discussion

2.1. UV Photoresponse of ZnO NWFET

We used transmission electron microscopy (TEM) and scanning transmission electron microscopy (STEM, JEOL JEM ARM 200F) to determine the crystal structure of the ZnO NWs. **Figures 1**a and b present low-magnification and high-resolution (HR) TEM images, respectively, of a ZnO NW. The lattice fringes have a spacing of 0.52 nm, corresponding to the lattice constant of (0001) ZnO, indicating *c*-axis growth of the ZnO NWs. We further investigated the atomic arrangement of ZnO NWs under aberration-corrected conditions. Figures 1c and d display annular dark field (ADF) and false-colored annular bright field (ABF) HR-STEM images, respectively, of a ZnO NW. Notably, ABF STEM imaging can provide clear information regarding the atomic arrangement of elements in materials.[15] Accordingly, we observe the ABABAB stacking order of wurtzite-structured ZnO along the <0001> direction in Figure 1d.

The upper-right inset to **Figure 2**a displays a representative structure of a back gate ZnO NWFET (see Experimental Section for device fabrication). The lower-right inset to Figure 2a presents a top-view scanning electron microscopy (SEM) image of an NWFET featuring an individual ZnO NW bridging two metal electrodes; the NW diameter (R_{NW}) is approximately 130 nm and its channel length (L_{NW}) is approximately 3.5 μm. Figure 1a displays the conductance characteristics of the ZnO NWFET with ohmic contacts plotted with respect to the gate voltage (V_G, ranging from –80 to +20 V) in an ambient environment. It suggests that altering the width of the surface

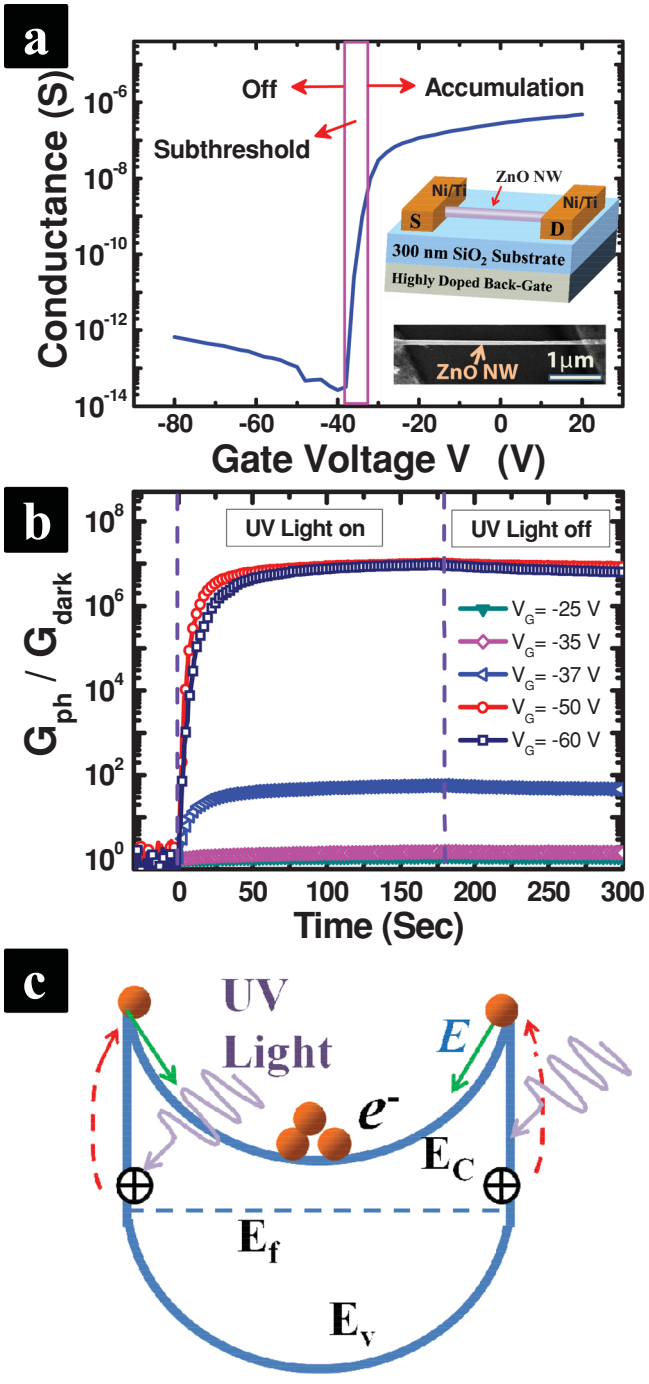

Figure 2. (a) NW conductance plotted with respect to the gate voltage (V_G, varied from –80 to +20 V). Upper-right inset: Representative structure of a back gate ZnO NWFET. Lower-right inset: top-view SEM image of an NWFET featuring a single ZnO NW (channel length: ca. 3.5 μm; NW diameter: ca. 130 nm). (b) Ratios of photoconductance (G_{ph}) to dark conductance (G_{dark}) under values of V_G of –25, –35, –37, –50, and –60 V, recorded in real-time. (c) Band diagram of the ZnO NW under UV illumination. E_c, E_v, and E_f represent the conduction band, valence band, and Fermi energy level, respectively, of the ZnO NW. The symbol ⊕ represents the positively charged defect. The large surface electric field (E) assisted the dissociation of photoexcited charges and then drove the free electrons toward the inner zone of the NW, leaving behind positively charged centers near the surface.

© 2014 WILEY-VCH Verlag GmbH & Co. KGaA, Weinheim

space-charge layer in the ZnO NW, through the application of different values of V_G, will effectively modulate the conductance from the off mode through subthreshold to accumulation modes.

To investigate the photoconductivity performance, we recorded the ratios of the photoconductance (G_{ph}) to the dark conductance (G_{dark}) of the NW in real-time under UV light exposure [power density (P_{UV}): 25.75 nW cm^{-2}] for 180 s at various values of V_G, as displayed in Figure 2b. Interestingly, we observed a giant magnitude of approximately 10^7 for G_{ph}/G_{dark} when we operated the ZnO NWFET in the off mode ($V_G \leq -50$ V). In contrast, the magnitude of G_{ph}/G_{dark} was approximately equal to 1 for the NWFET in the accumulation operation mode. Recent reports have described evident changes in the conductance of two-terminal ZnO NW diodes only when the NWs were exposed to high values of P_{UV} of at least several microwatts per square centimeter.[16] Hence, our finding of a giant value of G_{ph}/G_{dark}, spanning several orders of magnitude, at an ultralow value of P_{UV} appears to have great potential to facilitate the technological development of photosensitive elements for future optoelectronic applications.

After the termination of UV excitation, the photoconductivity exhibited a significantly slow recovery rate, implying that the PPC effect dominated the physical mechanism of the photoconductance in the ZnO NW. First-principles theoretical calculations suggested that neutral oxygen vacancies (V_O), which formed deep defect-localized states (DLS) in the ZnO bandgap and could be photoexcited to form a metastable defect configuration of the ionized 2+ state (V_O^{2+}), were responsible for the PPC effect in ZnO.[10] Thus, the slow recovery process could be attributed to electrons captured by the immobile positively charged states through a thermal activation process involving large lattice relaxation. Recently, a surface defect state located at 240 meV above the valence band was observed experimentally in the PPC of ZnO.[17] Further investigation will be required to provide more information concerning the atomic defect configuration and the properties of the intrinsic defects responsible for the PPC in ZnO NWs.

To obtain physical insight into the giant photoconductivity associated with the PPC in ZnO NWs, we investigated the dissociation rate of the photoexcited electron separated from the positively charged center. From the point of view of photodiodes,[18] the applied electric field in the space-charge region plays a decisive role in determining the dissociation rate of photoexcited charges. We estimated the surface potential (ϕ_s) of a fully depleted ZnO NW having a diameter of 130 nm to be approximately 2.2 eV when operating the NWFET in the off mode, resulting in a large surface electric field (E) of approximately 6.7×10^7 V m^{-1} (see Supporting Information, part S1). Regarding the effect of the applied electric field on the dissociation rate of photoexcited carriers,[19] it has been suggested, for ZnO, that if the electric field exceeds approximately 10^6 V m^{-1}, then the dissociation rate of a photoexcited electron bound by an attractive Coulomb potential, induced by positively charged states, will be greatly improved (Supporting Information, Figure S2). Under fully depleted conditions, the presence of a large surface electric field will cause photoexcited electrons bound by immobile positively charged states to more readily surmount the attractive Coulomb potential and move along the surface electric field toward the inner zone of the NW, leaving behind the immobile positively charged centers near the NW surface, as displayed in Figure 2c. Hence, the large surface electric field within the space-charge layer will assist the dissociations of photoexcited electrons and will also ensure the ultrahigh photosensitivity of the fully depleted ZnO NW.

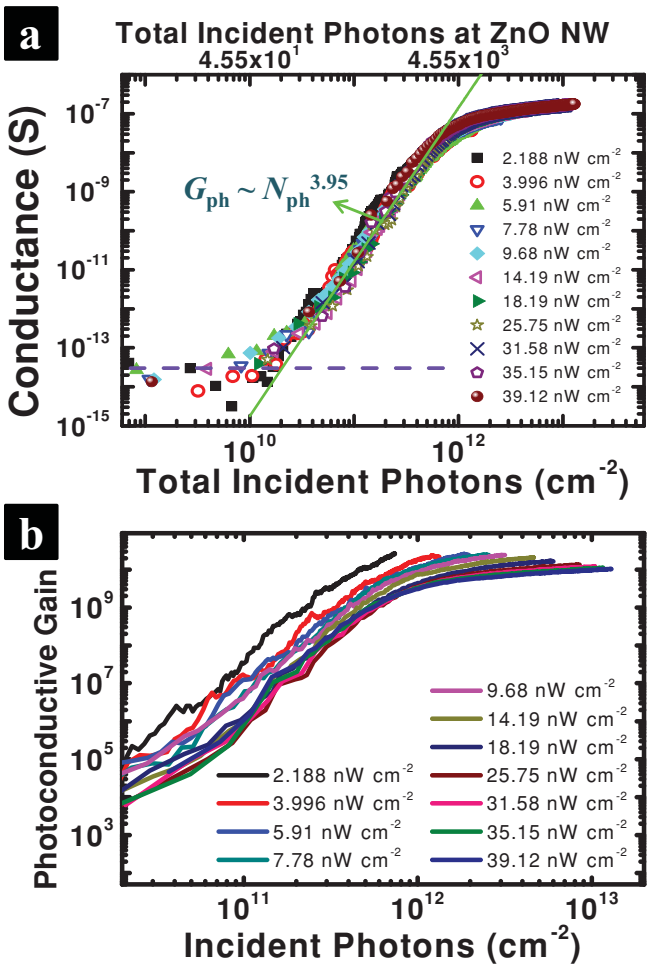

Figure 3. (a) Conductance of the NWFET plotted with respect to the total number of incident photons per unit area upon UV illumination at various power densities at a value of V_G of –50 V. The purple dashed line is the noise level of the NW conductance. A power law ($G_{ph} \sim N_{ph}^{3.95}$) was fitted to the experimental photoconductance in the low-N_{ph} regime (green solid line). For comparison, the units of the upper x-axis have been scaled to the number of photons incident on the NW. (b) Dynamic photoconductive gain plotted with respect to the total number of incident photons per unit area. The extremely high photoconductive gain (ca. 10^{10}) is physically ascribed to the modulation of the surface space-charge layer width after the accumulation of positively charged surface defects.

2.2. Ultrahigh Photoconductive Gain in ZnO NWFET

We have demonstrated that an NWFET operated in the off mode will result in a large surface electric field that will assist the dissociation of photoexcited charges. To provide a deeper understanding of the photoconductive characteristics of the fully depleted ZnO NW, **Figure 3**a displays the pho-

© 2014 WILEY-VCH Verlag GmbH & Co. KGaA, Weinheim

toconductance of the ZnO NWFET upon UV illumination at values of P_{UV} ranging from several to tens of nanowatts per square centimeter, plotted with respect to the total number of incident photon per unit area (N_{ph}), defined as

$$N_{ph} = P_{UV}t/h\nu \quad (1)$$

where t and $h\nu$ are the UV exposure time and photon energy, respectively. The conductance of the NW increased greatly upon increasing the value of N_{ph}, reaching almost saturated characteristics in photoconductance when N_{ph} exceeded approximately 10^{12} cm^{-2}. More importantly, the measured photoconductance of the ZnO NW under different values of P_{UV} appeared to follow the same trend with respect to N_{ph}, implying that the photoconductance strongly depended on the number of UV photons exposed to the NW. Furthermore, we used a typical power law to express the dependence of the photoconductance G_{ph} of the NW on the value of N_{ph} in the low-N_{ph} regime:

$$G_{ph} \sim N_{ph}\,3.95 \quad (2)$$

The fitting line obtained using Equation (2) is plotted as the green solid line in Figure 3a. Notably, the exponent (3.95) is much larger than unity, implying that the dynamic accumulation of positively charged defects near the NW surface would govern the photoconductance of the ZnO NW in terms of modulation of the surface space-charge width. In addition, when we scaled the value of N_{ph} to the number of incident photons at the NW surface, by multiplying N_{ph} by L_{NW} and R_{NW}, we found that the conductance of the fully depleted NW could be changed significantly when applying only a few hundred photons incident on the NW.

Figure 3b reveals that the dynamic photoconductive gain (g) reached up to approximately 10^{10}; we derived these values from the data in Figure 3a, obtained using the equation

$$g = (G_{ph} - G_{dark})V_D h\nu/q\eta R_{NW}L_{NW}P_{UV} \quad (3)$$

where q and V_D are the elementary charge and the applied drain voltage, respectively, and η is the efficiency of photon absorption in the NW, estimated to be as high as 0.65.[20] Note that the presence of a surface electric field exceeding a value on the order of 10^6 V m^{-1} in the fully depleted ZnO NW would significantly assist the rate of dissociation of the photoexcited charges near the NW surface, as described above. Thus, the surface density of immobile ionized defects accumulated near the NW surface could reach as high as approximately 10^{11} cm^{-2}, resulting in the extremely high dynamic photoconductive gain of approximately 10^{10} (see Supporting Information, part S3).

2.3. Multibit Programmable Optoelectronic NW Memory

The operating principle for electrical writing in charge-storage memories that are used widely in commercial electronic products (e.g., FLASH memories) involves charge carriers being injected into the empty trapping sites, typically by applying a high electric field between the channel and gate.[18] Accordingly, the trapped charges will locally modulate the surface potential of the conducting channel and deplete carriers in close proximity, resulting in decreased conductance, as depicted in **Figure 4**a,b; the profiles of the surface potential V_s at the dielectric–channel interface along the channel direction under thermal equilibrium for the initial and programming states are sketched as solid red lines. In a similar way, we attempted to utilize the surface photoionized defects, performing the role of the trapped charges in charge trapping memories, to realize an optical writing optoelectronic NW memory. Figures 4c and d provide schematic representations of the operating principle of such an optical writing NW memory, revealing that the surface space-charge width (W_{dep}) will narrow upon formation of positively charged surface defects under illumination with UV light. The spatial distributions of the band-bending potential drop V_b across the ZnO NW along the radial direction for the initial and programming states are represented as solid red lines. Note that the low degree of wavefunction overlap between the positively charged surface defect and the electron confined at the inner zone of NW will suppress the recombination rate, resulting in significantly slower recovery.

Taking advantage of the photoconductive features of the NW—the ultrahigh photon sensing, the extremely high photoconductive gain, and the significant PPC effect—enabled us to prepare an optoelectronic NW memory. **Figure 5**a reveals the performance of an optical-writing electrical-reading-erasing ZnO NW memory having a multibit data storage capacity of up to 8 bits at room temperature, with the positively charged defects that originated from photoexcitation serving as the storage charges for the memory. Each optical bit was written bit-by-bit into the NW through UV excitation at a value of P_{UV} of 3.996 nW cm^{-2} for 10 s, followed by a retention period of 50 s for electrical reading; the optical writing energy was ultralow, only approximately 180 aJ bit^{-1} (ca. 330 photons) for each optical bit. After termination of the optical writing signal, the magnitude of the photoconductance corresponding to each bit persisted as a result of the slow photoconductance recovery attributed to the significant PPC effect. Notably, we observed a change of at least 30% in the NW conductance, relative to that of the previous bit state, at a power density of 3.996 nW cm^{-2} in the higher data bit regime, as denoted by the red line in Figure 5b. From the viewpoint of modern electronics, a change of at least 30% in NW conductance in the higher conductance regime would be easy to identify when using commercial readout ICs.

For electrical erasing of the persistent photoconductance, we applied a positive gate voltage of 20 V to the NW memory to not only raise the Fermi energy level but also increase the electron density in the ZnO NW and, thereby, greatly enhance the probability of electron capture by positively charged defects through a thermal activation process.[8,12,21] After applying this high value of V_G for approximately 20 s, the conductance of the NW returned back to that in the initial state—that is, the change in conductance spanned more than six orders of magnitude. In addition, we estimated the standby power consumption in the NWFET, considering the contributions of each electrode terminal, to be less than 1 pW; this ultralow standby power consumption suggests potential applications as programmable optoelectronic elements in next-generation multifunctional nanochips. Relative to modern nanoFETs featuring ultrathin

© 2014 WILEY-VCH Verlag GmbH & Co. KGaA, Weinheim

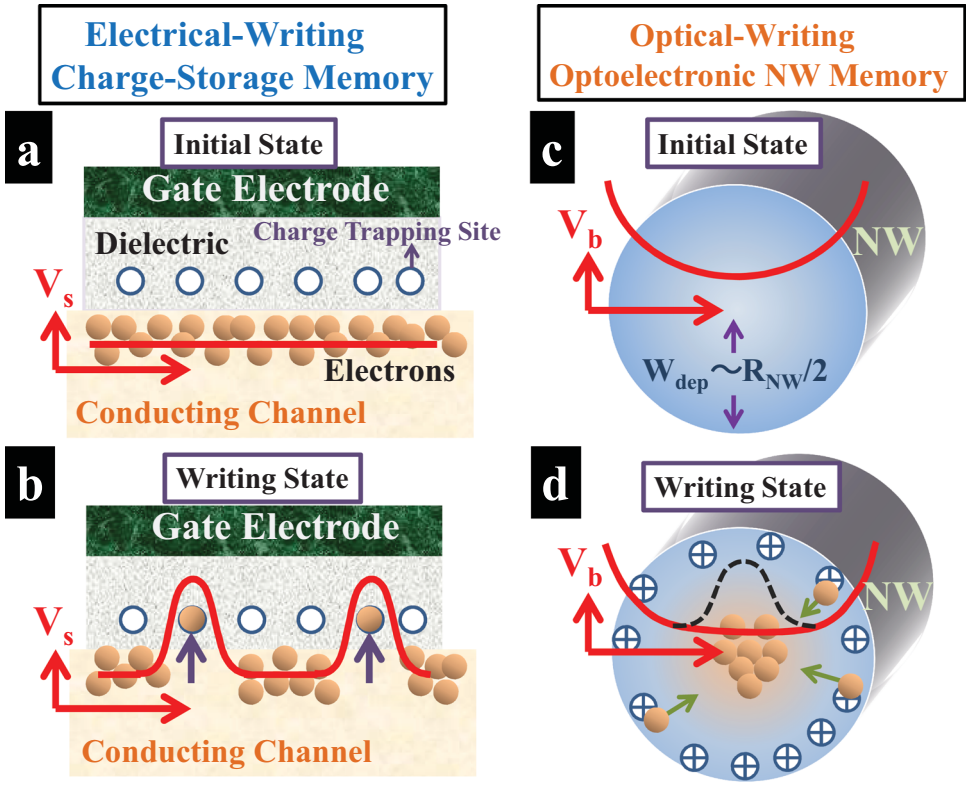

Figure 4. (a) Operating principle and surface potential profile of the electrical-writing charge-storage memory (e.g., FLASH or quantum dot memory) in the initial state. The profile of the surface potential V_S at the dielectric–channel interface along the channel direction is plotted as a red solid line. (b) Operating principle and surface potential profile of the charge-storage memory in the writing state. The profile of the surface potential (V_S) electrically deformed by the trapped charges along the channel direction is plotted as a red solid line. (c) Operating principle and band-bending potential drop (V_b) of the optical-writing NW memory in the initial state. The value of V_b across the fully depleted NW along the radial direction is plotted as a red solid line. (d) Operating principle and band-bending potential drop (V_b) of the optical-writing NW memory in the writing state. The value of V_b deformed by the surface charged defects is plotted as a red solid line. The symbol ⊕ represents the positively charged defects generated upon UV photoionization. The black dashed line is used to sketch the spatial distribution of free electron carriers confined by the band-bending potential profile.

gate dielectrics, the 300 nm–thick SiO_2 layer that served as the gate dielectric in our present study made it more difficult to use gated control to electrically modulate the carrier density in the NW; accordingly, a large gate voltage should be applied to electrically deplete or accumulate the electrons in the ZnO NW. We suspect, however, that if the thickness of gate dielectric were decreased to reach a level comparable with those in modern nanoFETs, the gate voltage required to perform data-writing or -erasing would scale reasonably to meet the requirements of the operation voltage in modern electronic chips.

To obtain greater insight into the dynamic equilibrium between the dissociation and recombination events in the NW, we applied UV light at various values of P_{UV} as a means of optical excitation to write optical data into the NW (Figure 5b). The optical writing period for each bit was maintained at 10 s, followed by a reading time of 50 s. When more positively charged defects and electrons were created upon UV excitation at a higher value of P_{UV}, the probability of electron capture by positively charged surface defects was augmented after terminating the optical signal. Figure 5c presents a semilogarithmic plot of the mean photoconductance for each programming bit, obtained through averaging of the measured photoconductance after termination of optical excitation. The inset to Figure 5b reveals linearity in the mean photoconductance of the ZnO NW, implying high feasibility for using NWFETs to perform linear optical computing. In Figure 5b, the real-time photoconductance of the NWFET under various UV power densities reveals dynamic equilibrium between the dissociation and recombination events in the NW. The typical recovery characteristics of the PCC effect, which can be described simply by an exponential decay law, were evident when we exposed the NW to UV excitation of higher power density, revealing that the recovery time constant, reflecting the rate of the recombination between electrons and positively photoionized centers, in the NW was at least a few tens of seconds. More importantly, the recovery in conductance of the NW was slower when the NW was exposed to UV excitation of low power density. Therefore, this optoelectronic NW memory has potential applications for transient optical data storage/buffering in future hybrid photonic-electronic circuits.

The rate of dissociation of photoexcited charges within the space-charge region is a critical parameter affecting the

© 2014 WILEY-VCH Verlag GmbH & Co. KGaA, Weinheim

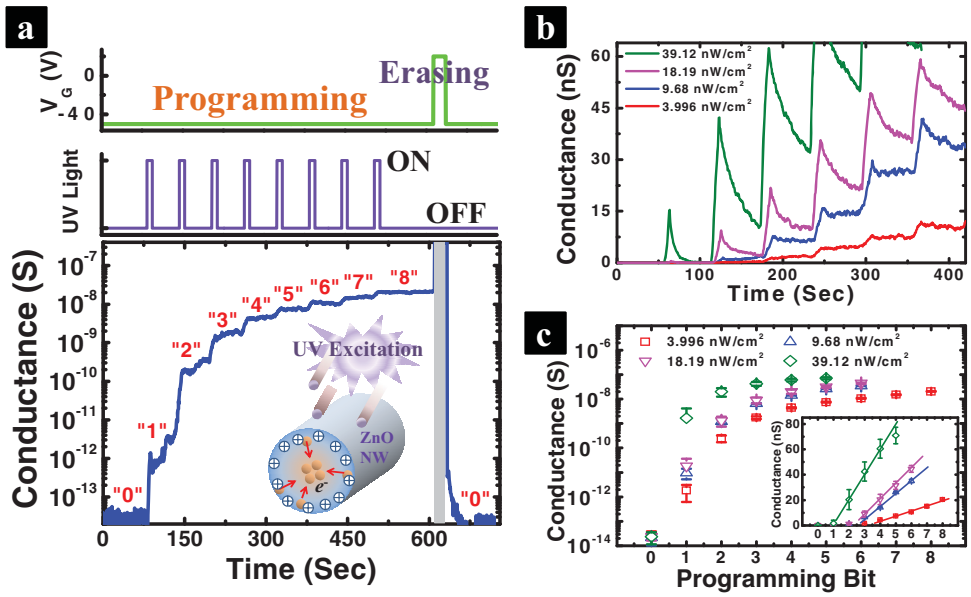

Figure 5. (a) An optical-writing/electrical-reading-erasing multibit programmable optoelectronic NW memory with capacity for optical data storage of up to 8 bits at room temperature. Upper figure: Memory programming at a value of V_G of –50 V and the 20-s period of erasing at a value of V_G of +20 V. Middle figure: Each optical bit was written into the NW through UV excitation at a value of P_{UV} of 3.996 nW cm^{-2} for 10 s, followed by a reading period of 50 s. Lower figure: Each optical signal of approximately 180 aJ bit^{-1} (ca. 330 photons) could be used to write data bit-by-bit into the NW, as denoted in the figure; inset: the symbol ⊕ represents the positively charged defects accumulated near the NW surface. After termination of the 8-bit optical writing process, the gate voltage was changed from –50 to +20 V for photoconductance erasing. (b) Real-time photoconductance of the NWFET under optical writing at various power densities. The optical writing period for each bit was 10 s, followed by a reading time of 50 s at a value of V_G of –50 V. (c) Semilogarithmic plot of the mean photoconductance at each programming bit, obtained by averaging the measured photoconductance after terminating optical excitation. Inset: Linearity in the plots of mean photoconductance; solid lines are merely guides for the eye.

photoconductive performance of photodiodes and optoelectronics. Especially for nanostructured materials that exhibit a strong surface effect, the surface space-charge layer significantly modulates the conductance and photoconductive characteristics.[22,23] In this study, we created a high surface electric field—as high as 6.7×10^7 V m^{-1}—in the fully depleted ZnO NW to greatly amplify the rate of dissociation of the photoexcited charges. Recently, Yang et al. found experimentally that the dielectric constant of a ZnO NW decreases upon narrowing its diameter, implying that the dielectric constant of the surface space-charge layer is much lower than that of bulk ZnO (8.66).[24] If we take into account the decrease in the dielectric constant of the space-charge layer of the ZnO NW, the surface electric field in the fully depleted ZnO NW would be enhanced; consequently, the rate of dissociation of the photoexcited charges in the surface space-charge layer of the ZnO NW would increase. Further investigation will be needed to determine the dielectric constants of surface space-charge layers in nanomaterials to be used for nano-optoelectronics and nanoelectronics. Notably, several reports have demonstrated that the photoconductive response time in a ZnO NW is on the scale of nanoseconds.[16,25] In addition, it has been observed that the PPC effect in metal-oxide transistors can be eliminated effectively using a 10-ns gate pulse.[12] Those reports confirm the possibility of high-speed operation of optoelectronic memories incorporating ZnO NWs.

2.4. Issues in Optoelectronic NW Memory: Toward Practical Applications

In this study, we developed an approach to utilize the internal PPC effect, without deposition of an additional photoexcited charge storage layer, to enhance the storage capacity of multibit optical data in a ZnO NWFET. In addition, PPC phenomena have been observed widely in a variety of semiconductor materials,[8–10] suggesting that interactions, involving lattice relaxation, between photoexcited carriers and defects are responsible for the slow recovery of the photoconductance. Therefore, this approach toward the realization of optoelectronic memory elements in high-density photonic-electronic circuits, using ZnO NWFETs, might also have promise when applied to other FET-based optical memories incorporating other nanostructured materials. Further optimization of the NW diameter, channel length, and doping concentration should enable single-photon memory, single-photon detection, and photon counting.

We also observed degradation of the photoconductive characteristics of the ZnO NWFET over time. Figure S4a presents the conductance of the as-fabricated device and that measured two months after fabrication; more active traps were generated naturally over time, due to device degradation, leading to poorer gate control. Consequently, the ZnO NWFET became less sensitive to UV excitation, as revealed in Figure S4b.

© 2014 WILEY-VCH Verlag GmbH & Co. KGaA, Weinheim

Note that we adopted an upside-down FET structure without any passivation layer, ensuring direct exposure of the NW to the ambient environment. As a result, the device characteristics of the ZnO NW memory degraded significantly over time. Previous reports have demonstrated that the fabrication of ZnO NW with a passivation layer not only eliminates the influence of water or gas molecules on the electrical characteristics of ZnO NWs[22,26] but also leads to improved device characteristics.[27] Accordingly, application of a thin passivation layer should provide a feasible route toward improving the stability and electrical performance of optoelectronic NW memories.

Modern electronic systems feature several types of memory devices—for electrical data storage/buffering functions in data processing—that have been widely investigated and developed in academic and industrial settings over many decades.[28] Depending on its distinctive features (e.g., programming energy per bit, cell size, operation speed, data retention, and endurance), each commercial memory device has been assigned to perform a typical role during electrical data processing. For instance, DRAM and FLASH memories, two different memories in terms of their data storage mechanisms and memory performance, are applied functionally for short-term data buffering and long-term data storage purposes, respectively, in electronic systems. Here, we have attempted to open up new opportunities for NWFETs as fundamental optical data storage/buffering elements to bridge the gap between electronics and photonics. Accordingly, this preliminary report of an optoelectronic NW memory device—featuring multibit data storage capacity, ultralow optical writing energy, and low standby power consumption—demonstrates, at the laboratory level, functions of optical data processing that might be useful in the next generation of functional photonic-electronic circuits. There remain, however, several performance issues that must be resolved if we are to progress with optoelectronic NW memories and, thereby, position them in a distinctive role for optical data processing in future hybrid photonic-electronic circuits.

3. Conclusions

We have developed a new multibit programmable optoelectronic NW memory, featuring an ultralow optical writing energy of approximately 180 aJ bit^{-1} (ca. 330 photons bit^{-1}) and a low standby power consumption (<1 pW), that can be operated at room temperature; in this device, photoionized charged defects behave as surface trapped charges to provide the electrical memory effect. As a result of creating a high surface electric field along the radial direction in the surface space-charge layer, the rate of dissociation of the photoexcited charges is greatly improved, thereby decreasing the optical writing energy in the optoelectronic memory. Moreover, the extremely high dynamic photoconductive gain (ca. 10^{10}) makes it possible to write optical data bit-by-bit into the NW. This finding could be a major step toward the realization of optoelectronic nanoelements in 3D highly integrated optoelectronic nanochips for optical data storage/buffering, optical data processing, and optical sensing purposes.

4. Experimental Section

Fabrication and Characterization of ZnO NWFETs: Among the various 1D semiconducting nanomaterials, ZnO NWs, which possess a large direct band gap (3.37 eV) and a high binding energy (60 meV), are widely considered as promising candidates for use in functional optoelectronics,[29] including UV nanosensors/switches,[3,30] UV nanoLEDs,[31,32] and nanolasers.[33] For that reason, a ZnO NW was used to realize an optical memory as a route toward nano-optoelectronics based fully upon ZnO nanomaterials.

Naturally n-type–doped ZnO NWs, several micrometers in length, were grown on an n-type Si (001) wafer through thermal vapor deposition without growth catalysts.[32,34] Briefly, a mixture of ZnO and graphite powder was placed in an alumina boat and positioned at the zone of the furnace at 1050 °C. The ZnO thin film–coated Si substrates were located horizontally inside the furnace at a pressure of 1.0×10^{-3} torr and the growth temperature was kept at 600 °C. After ZnO NW growth, TEM was used to identify the crystal structure and the growth direction of the ZnO NWs; it revealed a preferential [0001] growth direction (Figure 1). Subsequently, the vertically aligned ZnO NWs on the growth substrate were mechanically transferred onto the surface of the heavily doped Si wafer covered with a 300 nm thick SiO_2 dielectric. The highly doped Si substrate served as the gate (G) electrode in the NWFET to electrically tune the width of the space-charge layer as well as the electron carrier density in the NW. The patterns of the source (S) and drain (D) electrodes contacting the two ends of a single ZnO NW were defined using e-beam lithography. After definition of the S/D electrode patterns, Ni/Ti layers (50 nm Ti; 120 nm Ni) were deposited for ohmic contact, using an electron beam evaporation system followed by a lift-off process. An upside-down structure for the back-gate NWFET was adopted to ensure that the NW channel was directly exposed to the UV radiation, as illustrated in the upper-right inset to Figure 2a.

To estimate the electron carrier density (n_e) within the NW, the geometrical gate capacitance (C_G), considering the effect of the fringing electric field distributed spatially in the SiO_2 dielectric and air environment, was calculated by using the finite element method (FEM).[35] The value of n_e per unit length in a ZnO NW at a gate voltage of 0 V was calculated using the equation

$$n_e = C_G|V_{th}|/q \quad (4)$$

where C_G and V_{th} are the geometrical gate capacitance and the threshold voltage, respectively. Accordingly, the electron doping concentration (N_D) was determined to be approximately 5×10^{17} cm^{-3}.

Measurements of Conductance and Photoconductive Characteristics of ZnO NWFET: In all measurements, ZnO NWFETs were placed inside a metal box with good grounded shielding at room temperature (300 K). The conductance–voltage (*G*–*V*) characteristics of the ZnO NWFETs were recorded using a high-performance source meter (Keithley 2636A). The drain voltage (V_D) and gate voltage (V_G) were applied to the drain and gate electrodes of the NWFETs, respectively. The value of V_D was maintained at 2 V in all conductance measurements. The source electrode was connected to the ground terminal of the measurement system. To perform the photoconductance measurement, a commercial 365-nm UV LED was powered by a DC power supply (Agilent). The output light of the UV LED was filtered using a narrow bandpass filter (Newport). The incident direction of the UV light was perpendicular to the NWFET surface. To supply UV light at an ultralow level, a neutral density filter (Newport) was used to modulate the UV power density from several to tens of nanowatts per square centimeter. The UV power density was measured using a high-performance optical power meter (Newport 1918) equipped with low-power UV photodiodes (Newport 918D). Moreover, for measurements of the optical-writing, electrical-reading, and electrical-erasing memory, an automatic measurement system using Labview software was used to control all of the instruments involved. Because of the limited response time of this home-built measurement system, the time periods for optical writing and electrical erasing were set on the order of several seconds to obtain stable and reliable data.

© 2014 WILEY-VCH Verlag GmbH & Co. KGaA, Weinheim

Supporting Information

Supporting Information is available from the Wiley Online Library or from the author.

Acknowledgments

We thank the National Nano Device Laboratories (NDL) for helpful assistance during device fabrication. This study was supported financially by the National Science Council of Taiwan (no. NSC102–2221-E-492–009).

Received: November 14, 2013
Published online: January 28, 2014

[1] a) M. S. Gudiksen, L. J. Lauhon, J. Wang, D. C. Smith, C. M. Lieber, *Nature* **2002**, *415*, 617; b) Y. Li, F. Qian, J. Xiang, C. M. Lieber, *Mater. Today* **2006**, *9*, 18; c) R. Yan, D. Gargas, P. Yang, *Nature Photon.* **2009**, *3*, 569.
[2] a) M. C. McAlpine, R. S. Friedman, S. Jin, K. Lin, W. U. Wang, C. M. Lieber, *Nano Lett.* **2003**, *3*, 1531; b) Y. Huang, X. Duan, C. M. Lieber, *Small* **2004**, *1*, 142.
[3] H. Kind, H. Yan, B. Messer, M. Law, P. Yang, *Adv. Mater.* **2002**, *14*, 158.
[4] a) O. Hayden, R. Agarwal, C. M. Lieber, *Nature Mater.* **2006**, *5*, 352; b) C. Yang, C. J. Barrelet, F. Capasso, C. M. Lieber, *Nano Lett.* **2006**, *6*, 2929.
[5] a) B. Tian, X. Zheng, T. J. Kempa, Y. Fang, N. Yu, G. Yu, J. Huang, C. M. Lieber, *Nature* **2007**, *449*, 885; b) L. Li, T. Zhai, Y. Bando, D. Golberg, *Nano Energy* **2012**, *1*, 91.
[6] a) C. J. Barrelet, A. B. Greytak, C. M. Lieber, *Nano Lett.* **2004**, *4*, 1981; b) X. Guo, M. Qiu, J. Bao, B. J. Wiley, Q. Yang, X. Zhang, Y. Ma, H. Yu, L. Tong, *Nano Lett.* **2009**, *9*, 4515.
[7] a) A. Star, Y. Lu, K. Bradley, G. Grüner, *Nano Lett.* **2004**, *4*, 1587; b) J. Borghetti, V. Derycke, S. Lenfant, P. Chenevier, A. Filoramo, M. Goffman, D. Vuillaume, J. P. Bourgoin, *Adv. Mater.* **2006**, *18*, 2535; c) C. J. Kim, S. J. Choi, J. H. Ahn, J. W. Han, H. Kim, S. Yoo, Y. K. Choi, *ACS Nano* **2012**, *6*, 1449.
[8] D. V. Lang, R. A. Logan, *Phys. Rev. Lett.* **1977**, *39*, 635.
[9] J. Kakalios, H. Fritzsche, *Phys. Rev. Lett.* **1984**, *53*, 1602.
[10] S. Lany, A. Zunger, *Phys. Rev. B* **2005**, *72*, 035215.
[11] a) A. Janotti, C. G. Van de Walle, *Appl. Phys. Lett.* **2005**, *87*, 122102; b) A. Janotti, C. G. Van de Walle, *Phys. Rev. B* **2007**, *76*, 165202; c) S. E. Ahn, I. Song, S. Jeon, Y. W. Jeon, Y. Kim, C. Kim, B. Ryu, J. H. Lee, A. Nathan, S. Lee, *Adv. Mater.* **2012**, *24*, 2631.
[12] S. Jeon, S.-E. Ahn, I. Song, C. J. Kim, U.-I. Chung, E. Lee, I. Yoo, A. Nathan, S. Lee, J. Robertson, K. Kim, *Nature Mater.* **2012**, *11*, 301.
[13] K. Ghaffarzadeh, A. Nathan, J. Robertson, S. Kim, S. Jeon, C. Kim, U. I. Chung, J. H. Lee, *Appl. Phys. Lett.* **2010**, *97*, 143510.
[14] R. Chau, S. Datta, M. Doczy, B. Doyle, B. Jin, J. Kavalieros, A. Majumdar, M. Metz, M. Radosavljevic, *IEEE Trans. Nanotechnol.* **2005**, *4*, 153.
[15] R. Ishikawa, E. Okunishi, H. Sawada, Y. Kondo, F. Hosokawa, E. Abe, *Nature Mater.* **2011**, *10*, 278.
[16] C. Soci, A. Zhang, B. Xiang, S. Dayeh, D. Aplin, J. Park, X. Bao, Y. Lo, D. Wang, *Nano Lett.* **2007**, *7*, 1003.
[17] P. Liu, G. She, Z. Liao, Y. Wang, Z. Wang, W. Shi, X. Zhang, S. T. Lee, D. Chen, *Appl. Phys. Lett.* **2009**, *94*, 063120.
[18] S. Sze, Physics of Semiconductor Devices, John Wiley & Sons, New York **1981**.
[19] a) L. Onsager, *Phys. Rev.* **1938**, *54*, 554; b) D. Pai, R. Enck, *Phys. Rev. B* **1975**, *11*, 5163.
[20] Z. Zhang, X. Qi, J. Jian, X. Duan, *Micron* **2006**, *37*, 229.
[21] a) C. Henry, D. V. Lang, *Phys. Rev. B* **1977**, *15*, 989; b) M. P. Lu, M. J. Chen, *Phys. Rev. B* **2005**, *72*, 235417.
[22] W. K. Hong, J. I. Sohn, D. K. Hwang, S. S. Kwon, G. Jo, S. Song, S. M. Kim, H. J. Ko, S. J. Park, M. E. Welland, *Nano Lett.* **2008**, *8*, 950.
[23] R. Calarco, M. Marso, T. Richter, A. I. Aykanat, R. Meijers, A. vd Hart, T. Stoica, H. Lüth, *Nano Lett.* **2005**, *5*, 981.
[24] Y. Yang, W. Guo, X. Wang, Z. Wang, J. Qi, Y. Zhang, *Nano Lett.* **2012**, *12*, 1919.
[25] a) Q. Xu, J. Zhang, K. Ju, X. Yang, X. Hou, *J. Crystal Growth* **2006**, *289*, 44; b) K. Liu, J. Ma, J. Zhang, Y. Lu, D. Jiang, B. Li, D. Zhao, Z. Zhang, B. Yao, D. Shen, *Solid State Electron.* **2007**, *51*, 757; c) X. Bian, J. Zhang, Z. Bi, D. Wang, X. a. Zhang, X. Hou, *Opt. Eng.* **2008**, *47*, 064001.
[26] S. Song, W.-K. Hong, S.-S. Kwon, T. Lee, *Appl. Phys. Lett.* **2008**, *92*, 263109.
[27] P.-C. Chang, Z. Fan, C.-J. Chien, D. Stichtenoth, C. Ronning, J. G. Lu, *Appl. Phys. Lett.* **2006**, *89*, 133113.
[28] M. H. Kryder, C. S. Kim, *IEEE Trans. Magn.* **2009**, *45*, 3406.
[29] M. P. Lu, M. Y. Lu, L. J. Chen, *Nano Energy* **2012**, *1*, 247.
[30] J. Zhou, Y. Gu, Y. Hu, W. Mai, P. H. Yeh, G. Bao, A. K. Sood, D. L. Polla, Z. L. Wang, *Appl. Phys. Lett.* **2009**, *94*, 191103.
[31] X. M. Zhang, M. Y. Lu, Y. Zhang, L. J. Chen, Z. L. Wang, *Adv. Mater.* **2009**, *21*, 2767.
[32] M. T. Chen, M. P. Lu, Y. J. Wu, J. Song, C. Y. Lee, M. Y. Lu, Y. C. Chang, L. J. Chou, Z. L. Wang, L. J. Chen, *Nano Lett.* **2010**, *10*, 4387.
[33] a) M. H. Huang, S. Mao, H. Feick, H. Yan, Y. Wu, H. Kind, E. Weber, R. Russo, P. Yang, *Science* **2001**, *292*, 1897; b) S. Chu, G. Wang, W. Zhou, Y. Lin, L. Chernyak, J. Zhao, J. Kong, L. Li, J. Ren, J. Liu, *Nature Nanotechnol.* **2011**, *6*, 506.
[34] M. P. Lu, J. Song, M. Y. Lu, M. T. Chen, Y. Gao, L. J. Chen, Z. L. Wang, *Nano Lett.* **2009**, *9*, 1223.
[35] M. P. Lu, *Phys. Rev. B* **2012**, *86*, 045433.

© 2014 WILEY-VCH Verlag GmbH & Co. KGaA, Weinheim